Continuous Bed Motion in a Silicon Photomultiplier–Based Scanner Provides Equivalent Spatial Resolution and Image Quality in Whole-Body PET Images at Similar Acquisition Times Using the Step-and-Shoot Method

Kodai Kumamoto[1], Hideaki Sato[1], Yuji Tsutsui[2], Shinichi Awamoto[3], Yasuo Yamashita[3], Shingo Baba[4], and Masayuki Sasaki[5]

[1]Department of Health Sciences, Graduate School of Medical Sciences, Kyushu University, Fukuoka, Japan; [2]Department of Radiological Science, Faculty of Health Science, Junshin Gakuen University, Fukuoka, Japan; [3]Division of Radiological Technology, Department of Medical Technology, Kyushu University Hospital, Fukuoka, Japan; [4]Department of Clinical Radiology, Graduate School of Medical Sciences, Kyushu University, Fukuoka, Japan; and [5]Department of Health Sciences, Faculty of Medical Sciences, Kyushu University, Fukuoka, Japan

This study investigated the spatial resolution and image quality of the continuous-bed-motion (CBM) method in a sensitive silicon photomultiplier–based PET/CT system compared with the traditional step-and-shoot (SS) method. **Methods:** A PET/CT scanner was used in this study. Data acquisition using the SS method was performed for 3 min per bed position. In the CBM method, the bed speed ranged from 0.5 to 3.3 mm/s. The acquisition time equivalent to the SS method was 1.1 mm/s for 2-bed-position ranges and 0.8 mm/s for 7-bed-position ranges. The spatial resolution was investigated using ^{18}F point sources and evaluated using the full width at half maximum. Image quality was investigated using a National Electrical Manufacturers Association International Electrotechnical Commission body phantom with 6 spheres 10, 13, 17, 22, 28, and 37 mm in inner diameter. The radioactivity concentration ratio of the ^{18}F solution in all spheres and the background was approximately 4:1. The detectability of each sphere was visually evaluated using a 5-step score. Image quality was physically evaluated using the noise-equivalent count rate, contrast percentage of the 10-mm hot sphere, background variability percentage, and contrast-to-noise ratio. **Results:** The spatial resolution was not affected by the difference in acquisition methods or bed speeds. The detectability of the 10-mm sphere with a bed speed of 2.2 mm/s or faster was significantly inferior to that of the SS 2-bed-position method. In evaluating image quality, we observed no significant difference in contrast percentage among the acquisition methods or speeds in the CBM method. However, the increasing bed speed in the CBM method increased the background variability percentage and decreased the noise-equivalent count rate. When comparing the SS 2-bed-position method with the CBM method at 0.8 mm/s, we observed no significant differences in any parameters. **Conclusion:** In whole-body PET images obtained with a silicon photomultiplier–based PET/CT scanner, the CBM method provides spatial resolution and image quality equivalent to the SS method, with the same acquisition time.

Key Words: continuous bed motion; step-and-shoot; SiPM; spatial resolution; image quality

J Nucl Med Technol 2022; 50:335–341
DOI: 10.2967/jnmt.121.263240

The step-and-shoot (SS) method has traditionally been used for PET data acquisition; however, the continuous bed motion (CBM) method was recently developed. In the SS method, multibed data are sequentially acquired only when the bed is stationary, not when the bed is moving (*1–10*). More than 1 min is wasted in a whole-body acquisition. Moreover, the axial acquisition range is determined by the number of bed positions, resulting in an unnecessary acquisition range and radiation exposure in a CT scan. In the CBM method, the bed continuously moves to acquire data (*2–10*), the axial acquisition range can be determined in a 0.1-mm unit, and the bed speed can be changed according to the body part (*2,3,6,8,9*). Moreover, generating a whole-body image by adding several fast whole-body scans should be useful if an examination is interrupted by patient motion or pain (*7,11*). It has been reported that patients preferred continuous bed movements over SS movements (*6*). Therefore, the CBM method may replace the SS method because of the flexibility of the PET examination for each patient. The usefulness of the CBM method in PET/CT using a photomultiplier tube system has been studied (*2–11*). Differences between the SS and CBM methods did not significantly affect SUV_{max} or SUV_{mean} in phantoms or tumors in clinical examinations (*3,4,6–9*). In contrast, the SS method has been reported to be superior to the CBM method in terms of variability in the background region (*4,9*).

Silicon photomultipliers (SiPMs), which are a type of semiconductor detector, were recently applied instead of the traditional photomultiplier tube in PET/CT scanners (*12–14*). Compared with conventional photomultiplier tube–based

Received Sep. 27, 2021; revision accepted Mar. 23, 2022.
For correspondence or reprints, contact Masayuki Sasaki (sasaki.masayuki.165@m.kyushu-u.ac.jp).
Published online Apr. 19, 2022.
COPYRIGHT © 2022 by the Society of Nuclear Medicine and Molecular Imaging.

PET scanners, SiPM-based PET scanners achieved a high gain and faster time response. This feature improves the sensitivity and time-of-flight timing resolution, thus resulting in good image quality, a short examination time, and a decrease in administered dose and radiation exposure (*15–17*). With these advantages, the CBM method using SiPM-based PET/CT scanners is expected to provide the same sufficient image quality with flexible examinations. However, the usefulness of the CBM method in SiPM-based PET/CT scanners has not been studied.

In this study, we investigated the image quality of the CBM method compared with the conventional SS method in SiPM-based PET/CT systems. Moreover, we evaluated the influence of varying bed speeds on image quality.

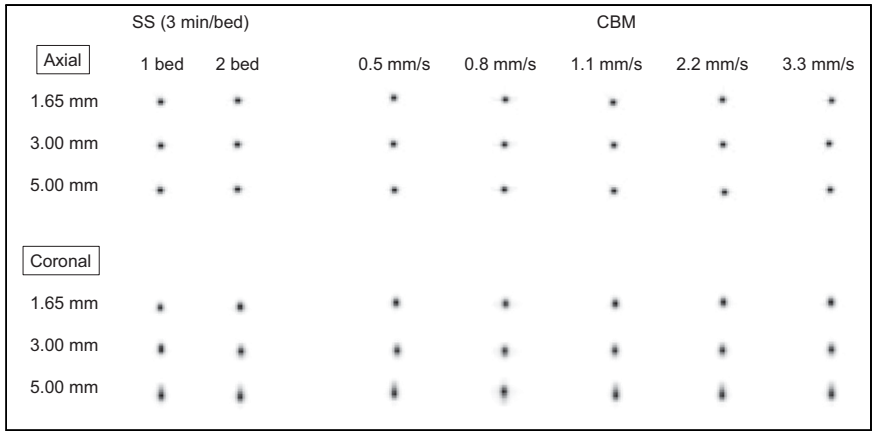

FIGURE 1. PET images of point source at coordinates (0,1) cm. Upper figure shows axial images, and lower one shows coronal images. No visual difference was observed among acquisition methods, whereas coronal images extended along with increase in slice thickness.

MATERIALS AND METHODS

PET/CT Scanner

PET data were acquired using a Biograph Vision PET/CT scanner (Siemens Healthineers). The PET system has 8 rings based on 38 detector blocks with lutetium oxyorthosilicate (Lu_2SiO_5:Ce) crystals (3.2 × 3.2 × 20 mm) and 6,400 crystals per ring. The transverse field of view was 700 mm, and the axial field of view was 263 mm. The spatial resolution at 1 cm was 3.7 mm in full width at half maximum (FWHM). The time-of-flight timing resolution was 214 ps, and the coincidence time window was 4.7 ns. These values were reported by the manufacturer. The CT system has 64 rows, and the rotation time was 0.33 s. CT images can be obtained using the following parameters: 70–120 kV, 20–666 mA, 0.5-s tube rotation, 0.8 pitch, and a 0.6-mm slice collimation. In this study, the voltage was 120 kVp and the tube current was set by CT automatic exposure control.

Point Source Phantom

The spatial resolution was investigated using ^{18}F point sources. One microliter of ^{18}F solution was put into glass capillaries with an inner diameter of 0.70 mm and an outer diameter of 0.97 mm. The radioactivity concentration was 30 MBq/mL. Point sources were placed at transaxial positions (1, 0), (10, 0), and (0, 10) cm on the same *z*-position.

Body Phantom

Image quality was investigated using a National Electrical Manufacturers Association (NEMA) International Electrotechnical Commission body phantom (Data Spectrum Corp.) with 6 spheres of 10-, 13-, 17-, 22-, 28-, and 37-mm inner diameter. The body phantom was an acrylic phantom that mimicked the torso of a human weighing 60 kg. The body phantom had a long diameter of 300 mm, a short diameter of 230 mm, a circumference of 840 mm, a height of 180 mm, and a volume of 9.7 L (Supplemental Fig. 1; supplemental materials are available at http://jnmt.snmjournals.org). The radioactivity concentration of ^{18}F solution in all spheres and the background was approximately 10.6 and 2.65 kBq/mL (ratio of 4:1), respectively. The radioactivity concentration was measured using an automatic well γ-counter (AccuFLEX γ7001; Hitachi Aloka Medical, Ltd.).

Data Acquisition and Image Reconstruction

In the SS method, data are acquired for 3 min/bed position × 1 bed position and 3 min/bed position × 2 bed positions in list mode according to the paper by Tsutsui et al. (*15*). The 1-bed-position acquisition was for the standard acquisition, whereas the 2-bed-position acquisition was for the overlapping acquisition. The overlap in multibed acquisitions was 49.8%, as determined by the manufacturer to improve the sensitivity distribution in the *z*-axis. In the CBM method, bed speeds of 0.5, 0.8, 1.1, 2.2, and 3.3 mm/s were investigated. Whole-body acquisition from the top of the head to the mid thigh usually require 7 or 8 bed positions in the standard SS method among Japanese institutions. The regional acquisition time of 0.8 mm/s in the CBM method was consistent with that of 8-bed acquisition at 3 min/bed position in the SS method. The 1.1 mm/s bed speed was consistent with a 2-bed-position acquisition at 3 min/bed position in the SS method.

In the spatial resolution investigation, PET images were reconstructed using filtered backprojection. The image matrix was 440 × 440 (1.65 × 1.65 mm), and the slice thicknesses were 1.65, 3.00, and 5.00 mm. Attenuation and scattering corrections were not used. In the image-quality investigation, PET images were reconstructed using ordered-subsets expectation maximization with point-spread-function correction and time-of-flight information. This study used 3 iterations and 5 subsets for the NEMA body phantom. Three iterations were done in accordance with our previous report (*15*). The Biograph Vision uses 5 subsets by default; this is fixed by the manufacturer and is unchangeable. CT attenuation correction was performed. Scatter correction was performed using single-scatter simulation. A gaussian filter was not used. The image matrix was 440 × 440, and the slice thickness was 1.65 mm.

Measurement of Spatial Resolution

The spatial resolution was evaluated using the FWHM. Profile curves of each point source in the *x-*, *y-*, and *z*-directions were created passing through the highest-count pixel on the highest-count slice using ImageJ (National Institutes of Health). In the profile curve, the maximum count was determined by a parabolic approximation using 1 point with the highest pixel count and 2 adjacent points. The FWHM of the 3 directions in each position was calculated by linearly interpolating between adjacent pixels at half the maximum value of the response function. FWHM $x_{(a,b)}$ is FWHM in the *x*-direction at

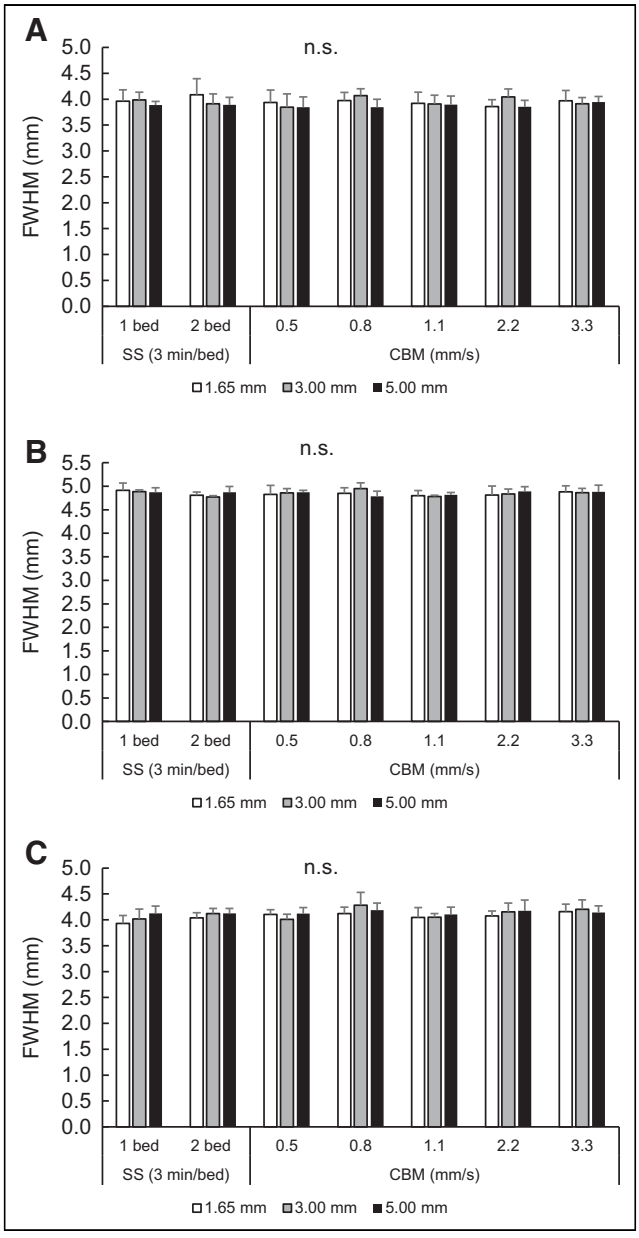

FIGURE 2. Comparison of FWHMs in axial plane of 1 cm radial (A), 10 cm radial (B), and 10 cm tangential (C). They did not significantly differ between SS and CBM methods or among different bed speeds in CBM method even when slice thickness was changed. n.s. = not statistically significant.

position (a,b). The spatial resolution was evaluated using a FWHM of 1 cm in the transverse direction, 10 cm in the transverse radial direction, and 10 cm in the transverse tangential and axial directions. These were calculated using the following equations:

- $\mathrm{FWHM}_{1\ \mathrm{cm}} = \{\mathrm{FWHM}\ x_{(0,1)} + \mathrm{FWHM}\ y_{(0,1)}\}/2$
- $\mathrm{FWHM}_{10\ \mathrm{cm\ radial}} = \{\mathrm{FWHM}\ x_{(10,0)} + \mathrm{FWHM}\ y_{(0,10)}\}/2$
- $\mathrm{FWHM}_{10\ \mathrm{cm\ tangential}} = \{\mathrm{FWHM}\ y_{(10,0)} + \mathrm{FWHM}\ x_{(0,10)}\}/2$
- $\mathrm{FWHM}_{\mathrm{axial}} = \{\mathrm{FWHM}\ z_{(0,1)} + \mathrm{FWHM}\ z_{(0,10)} + \mathrm{FWHM}\ z_{(10,0)}\}/3.$

Assessment of Image Quality

The detectability of each sphere was visually evaluated using a 5-step score (1, not absolutely visualized; 2, may not be visualized; 3, uncertain; 4, may be visualized; and 5, absolutely visualized) by a board-certified nuclear medicine physician and 2 radiologic technologists. Scores were averaged for each sphere. Fukukita et al. reported that they decided to use the score of the 10-mm sphere as the reference value because image quality and spatial resolution are most affected by the ability to visualize the 10-mm sphere (*18*). Therefore, we evaluated the visual scores of mainly the 10-mm sphere. Interobserver agreement was evaluated using the κ-coefficient.

In the NEMA body phantom PET images, the slice in which the hot sphere was most clearly observed was designated as the center slice. A region of interest (ROI) on the 10-mm hot sphere was placed in the center slice with the same inner diameter. Twelve circular ROIs with diameters of 10 and 37 mm were placed in the background on the center slice at ±1 cm and ±2 cm from the center slice (60 ROIs in total). According to the phantom test procedure for whole-body PET imaging with ^{18}F-FDG (*18*), the noise-equivalent counts, contrast percentage of the 10-mm hot sphere, background variability percentage, and contrast-to-noise ratio were calculated using the following equations. True, scatter, and random coincidences were acquired from a sinogram header, and the scatter fraction and random scaling factor were acquired from a default value. These processes were performed using PMOD software (version 3.8; PMOD Technologies LLC).

$$\mathrm{NEC}_{\mathrm{phantom}} = (1-SF)^2 \frac{(T+S)^2}{(T+S)+(1+k)fR}\ (\mathrm{Mcounts})$$
$$f = \frac{S_a}{\pi r^2},$$

where $\mathrm{NEC}_{\mathrm{phantom}}$ is the noise-equivalent counts and *T, S,* and *R* correspond to true, scatter, and random coincidences acquired within the scanning period, respectively. Moreover, *SF* and *k* are the scatter fraction and random scaling factor, respectively. The scatter fraction of Biograph Vision scanners is fixed at 0.39 by the manufacturer. The *k* is set to 0 because we used variance reduction techniques for estimating a smooth random distribution (*18*). The *f* is the ratio of object size to field of view. S_a is the cross-sectional area of the phantom. Finally, *r* is the radius of the detector ring diameter.

$$\mathrm{Q}_{H,\ 10\ \mathrm{mm}} = \frac{C_{H,\ 10\ \mathrm{mm}}/C_{B,\ 10\ \mathrm{mm}} - 1}{a_H/a_B - 1} \times 100\ (\%),$$

where $C_{H,\,10\,\mathrm{mm}}$ is the average count in the ROI for a 10-mm sphere, $C_{B,\,10\,\mathrm{mm}}$ is the average count of the 60 background ROIs of 10-mm diameter, and a_H and a_B are the radioactivity concentrations in the hot sphere and background, respectively.

$$N_{10\ \mathrm{mm}} = \frac{SD_{10\ \mathrm{mm}}}{C_{B,\ 10\ \mathrm{mm}}} \times 100\ (\%)$$
$$SD_{10\ \mathrm{mm}} = \sqrt{\sum_{k=1}^{K} (C_{B,\ 10\,\mathrm{mm},\ k} - C_{B,\ 10\ \mathrm{mm}})^2/(K-1)}, K = 60,$$

where $SD_{10\,\mathrm{mm}}$ is the SD of the background ROIs of 10-mm diameter and $N_{10\,\mathrm{mm}}$ is the background variability percentage (contrast-to-noise ratio):

$$Q_{10\ \mathrm{mm}}/N_{10\ \mathrm{mm}}.$$

Statistical Analysis

JMP Pro, version 15 (SAS Institute Inc.), was used for statistical analysis. The Tukey test was used to analyze the significance of the differences between the SS 2-bed-position method and the

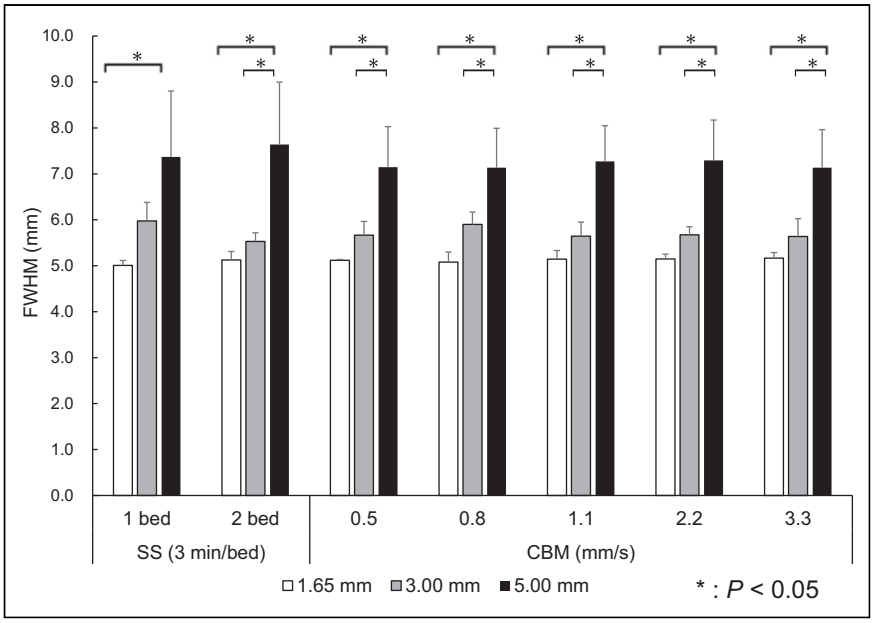

FIGURE 3. Comparison of FWHMs of body axial direction. They did not significantly differ among different acquisition methods and bed speeds, whereas FWHM significantly increased in thicker slices.

CBM method at each bed speed. *P* values of less than 0.05 were used to denote statistical significance.

RESULTS

Comparison of the Spatial Resolution

Figure 1 shows the PET images of point sources at position (0,1) cm. In the axial images, the shape and size did not differ among acquisition methods or bed speeds. In the coronal images, the image extended in the body axis direction in association with an increase in slice thickness. However, no differences in shape or size were seen among the different bed speeds.

Figure 2 shows the FWHM of the *x*- and *y*-directions. No significant differences in the 1-cm FWHM, 10-cm radial FWHM, or 10-cm tangential FWHM were observed between the SS and CBM methods. Moreover, the difference in the FWHM results when varying the slice thickness was insignificant. Figure 3 shows the axial FWHM. As the slice thickness increased, the axial FWHM significantly increased. However, no significant difference in the axial FWHM was observed between the SS and CBM methods or among the various bed speeds in the CBM method.

Assessment of Image Quality

Figure 4 shows the PET images of the NEMA body phantom in the SS and CBM methods. In the SS method, the clarity of the hot spheres and background variability were not visually different between 1-bed-position and 2-bed-position acquisitions. In the CBM method, the background variability increased as the bed speed increased. Figure 5 shows the results of the visual evaluation. The detectability of the 10-mm sphere with bed speeds faster than 2.2 mm/s was significantly inferior to that with the SS 2-bed-position method ($P < 0.05$). In the SS method, the score of the 10-mm sphere was above 4. In the CBM method, the bed speed should be 1.1 mm/s or slower to exceed the 10-mm sphere score of 3. Interobserver agreement was moderate ($\kappa = 0.55$).

Figure 6 compares the noise-equivalent counts. In the CBM method, the noise-equivalent counts decreased as the bed speed increased. The noise-equivalent counts in the CBM method with a bed speed of 1.1 mm/s or faster were significantly inferior to those in the SS 2-bed-position method ($P < 0.05$). Figure 7 shows the results of the physical assessment of image quality. No significant difference in contrast percentage of the 10-mm hot sphere was observed between the SS and CBM methods or among the various bed speeds in the CBM method (Fig. 7A). Figure 7B compares the background variability percentage. In the SS method, no difference in background variability percentage was observed between 1-bed-position and 2-bed-position acquisitions. In the CBM method, background variability percentage increased as bed speed increased. The background variability percentage in the CBM method with bed speeds of 1.1 mm/s or faster was significantly inferior to that in the SS 2-bed-position method ($P < 0.05$). Figure 7C compares the contrast-to-noise ratio. The contrast-to-noise ratio did not differ within the SS method, whereas in the CBM method, it decreased as the bed speed increased. The contrast-to-noise ratio in the CBM method with bed speeds of 2.2 mm/s or faster was significantly lower than that in the SS 2-bed-position method ($P < 0.05$).

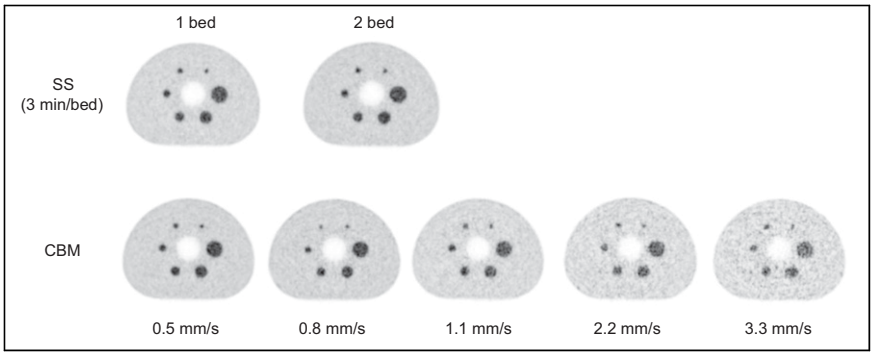

FIGURE 4. PET images of body phantom using SS method (top) and CBM method (bottom). In CBM method, images with faster bed speeds show high background variability.

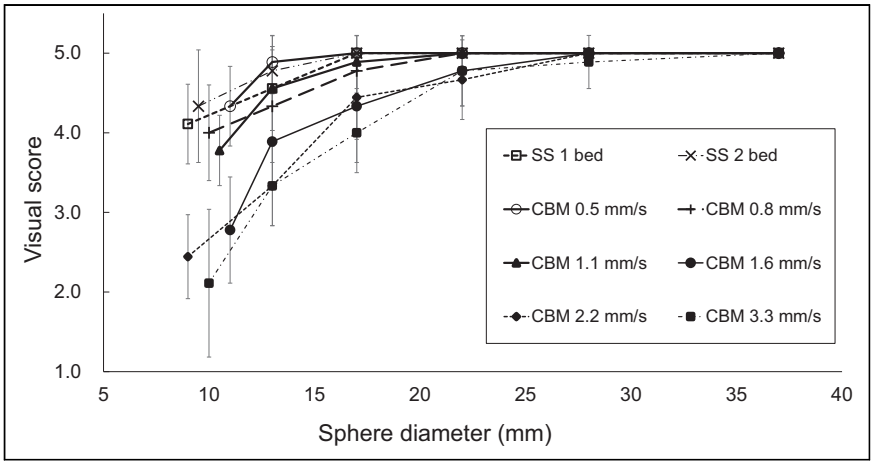

FIGURE 5. Visibility of hot spheres. Visual score of 10-mm sphere does not differ between SS 2-bed-position acquisition and 0.8 mm/s of CBM method. In CBM method, visual score decreased as bed speed increased.

DISCUSSION

Using the SiPM-based PET/CT scanner, the spatial resolution did not significantly differ between the SS and CBM methods or among the different bed speeds in the CBM method even when the slice thickness was changed. The noise-equivalent counts decreased as the bed speed increased in the CBM method. In assessing image quality, we found that the background variability significantly increased as the bed speed increased. However, the contrast of the hot sphere did not differ among acquisition methods or bed speeds.

The spatial resolution did not significantly differ between the SS and CBM methods or among the bed speeds in the CBM method. In the coronal planes, the FWHM increased as the slice thickness increased, but no significant difference was observed between the acquisition methods or among the different bed speeds. Because the PET data were acquired during continuous movement in the CBM method, image blurring was considered to increase the body axial FWHM. Furthermore, the increase in bed speed was also considered to exacerbate the spatial resolution. In the CBM method, when the bed position was shifted by a distance equal to the separation between sinogram planes, the events from the same detector were assigned to the next image plane. In the scanner used in this study, the CBM method data were separated and organized by the same axial sampling of 1.65 mm as in the SS method (*5*). Objects smaller than the pixel size were distributed uniformly over the entire pixel rather than at the center of the pixel. Thus, no significant difference was observed when the bed speed was changed by this function. In the transverse slice, the FWHM did not change when the slice thickness was increased because the pixel sizes were all the same.

The noise-equivalent counts using the NEMA body phantom showed no significant difference between the SS 2-bed-position acquisition and 0.8 mm/s using the CBM method. The noise-equivalent counts decreased as the bed speed increased. Because the acquisition time decreased as the bed speed increased, the noise-equivalent counts decreased because of reduced coincidence counts. This result is consistent with that reported previously (*7,15*). The background variability also increased as the bed speed increased. The increase in variability with decreasing counts is consistent with that reported previously (*15,19*). Regarding background variability, the SS method on the photomultiplier tube– based scanner was significantly superior to the CBM method using the same acquisition time (*4,9*). In contrast, that of the SS method was comparable to that of the CBM method on the SiPM-based scanner in this study. The improvement of the scanner's sensitivity and extension of the axial field of view in the SiPM system in this study is considered to improve the image quality of the CBM method. The visibility of the 10-mm hot sphere did not differ between the SS 2-bed-position acquisition and 0.8 mm/s using the CBM method, and the visual score decreased as the

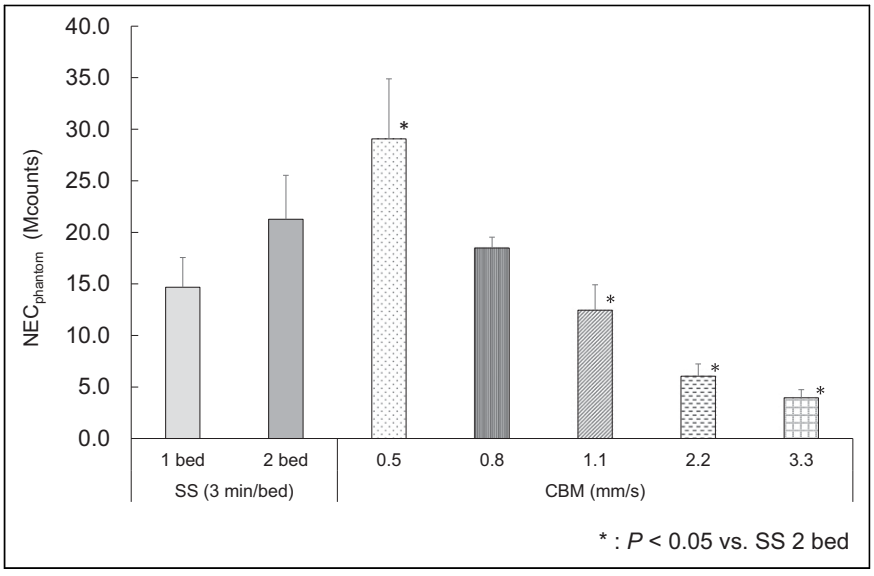

FIGURE 6. Noise-equivalent counts of SS and CBM methods. In CBM method, noise-equivalent counts significantly decreased as bed speed increased. Bed speeds of 1.1 mm/s or faster showed significantly inferior noise-equivalent count to that in SS 2-bed-position method. $NEC_{phantom}$ = noise-equivalent counts.

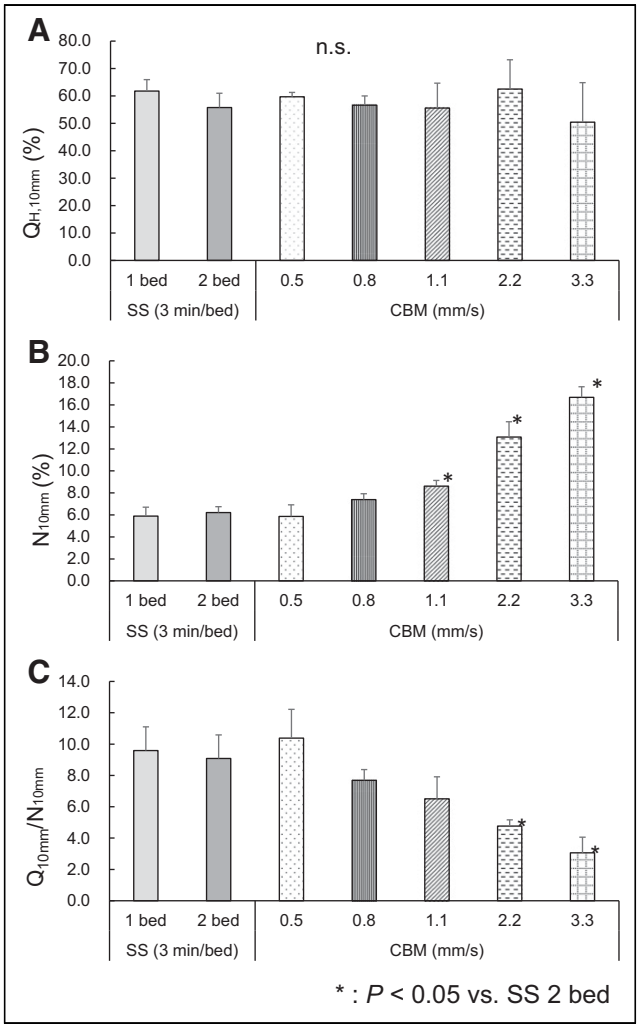

FIGURE 7. Physical assessment of PET image quality of SS and CBM methods. (A) Contrast percentage of 10-mm hot sphere did not significantly differ between SS and CBM methods or among different bed speeds in CBM method. (B) Bed speeds of 1.1 mm/s or faster showed background variability percentage significantly inferior to that in SS method. (C) Contrast–noise ratio in CBM method with bed speeds of 2.2 mm/s or faster was significantly lower than that in SS 2-bed-position method. N_{10mm} = background variability percentage; $Q_{H,10mm}$ = contrast percentage of 10-mm hot sphere; $Q_{H,10mm}/N_{10mm}$ = contrast-to-noise ratio.

bed speed increased. This is probably due to the increase in noise caused by the decrease in coincidence counts (*20*). The contrast values remained the same at all bed speeds. This tendency was also shown in a past study (*9,15*).

This study had some limitations. First, the number of bed speeds examined was limited. An examination with further varieties in bed speeds might reveal the appropriate bed speed equivalent to the SS method. Second, the CBM method was performed in only a single way. The image quality of the summed to-and-fro pass images should be examined. Third, the axial sampling size was fixed at 1.65 mm. A smaller axial sampling size may improve axial spatial resolution. Lastly, further clinical examinations should be conducted to compare the SS and CBM methods.

CONCLUSION

For SiPM-based PET/CT systems, image quality metric results were comparable between the SS method for 3 min/bed position and the CBM method for speeds of 0.8 mm/s at almost the same acquisition time in whole-body acquisitions. It is expected that the CBM method will be chosen in some cases depending on the combination of bed speeds.

DISCLOSURE

No potential conflict of interest relevant to this article was reported.

ACKNOWLEDGMENTS

We thank Kyushu University Hospital and its nuclear medicine and PET center team for allowing the use of their equipment and radioactive material.

KEY POINTS

QUESTION: Can the CBM method preserve the spatial resolution and image quality of the traditional SS method in an SiPM PET/CT scanner?

PERTINENT FINDINGS: No difference in spatial resolution or image quality was observed between the SS method and the CBM 0.8 mm/s method at similar acquisition times in whole-body acquisitions.

IMPLICATIONS FOR PATIENT CARE: Since the CBM method preserves the same image quality as the SS method and provides a more flexible examination, it is expected to be widely used in future when whole-body acquisitions are performed with semiconductor PET/CT systems.

REFERENCES

1. Dahlbom M, Hoffman EJ, Hoh CK, et al. Whole-body positron emission tomography: part I. Methods and performance characteristics. *J Nucl Med.* 1992;33:1191–1199.
2. Acuff SN, Osborne D. Clinical workflow considerations for implementation of continuous-bed-motion PET/CT. *J Nucl Med Technol.* 2016;44:55–58.
3. Osborne DR, Acuff S, Cruise S, et al. Quantitative and qualitative comparison of continuous bed motion and traditional step and shoot PET/CT. *Am J Nucl Med Mol Imaging.* 2014;5:56–64.
4. Rausch I, Cal-González J, Dapra D, et al. Performance evaluation of the Biograph mCT Flow PET/CT system according to the NEMA NU2-2012 standard. *EJNMMI Phys.* 2015;2:26.
5. Panin VY, Smith AM, Hu J, Kehren F, Casey ME. Continuous bed motion on clinical scanner: design, data correction, and reconstruction. *Phys Med Biol.* 2014;59:6153–6174.
6. Schatka I, Weiberg D, Reichelt S, et al. A randomized, double-blind, crossover comparison of novel continuous bed motion versus traditional bed position whole-body PET/CT imaging. *Eur J Nucl Med Mol Imaging.* 2016;43:711–717.

7. Yamamoto H, Takemoto S, Maebatake A, et al. Verification of image quality and quantification in whole-body positron emission tomography with continuous bed motion. *Ann Nucl Med.* 2019;33:288–294.
8. Meier JG, Erasmus JJ, Gladish GW, et al. Characterization of continuous bed motion effects on patient breathing and respiratory motion correction in PET/CT imaging. *J Appl Clin Med Phys.* 2020;21:158–165.
9. Yamashita S, Yamamoto H, Nakaichi T, Yoneyama T, Yokoyama K. Comparison of image quality between step-and-shoot and continuous bed motion techniques in whole-body ^{18}F-fluorodeoxyglucose positron emission tomography with the same acquisition duration. *Ann Nucl Med.* 2017;31:686–695.
10. Siman W, Kappadath SC. Comparison of step-and-shoot and continuous-bed-motion PET modes of acquisition for limited-view organ scans. *J Nucl Med Technol.* 2017;45:290–296.
11. Osborne DR, Acuff S. Whole-body dynamic imaging with continuous bed motion PET/CT. *Nucl Med Commun.* 2016;37:428–431.
12. Rausch I, Ruiz A, Valverde-Pascual I, Cal-González J, Beyer T, Carrio I. Performance evaluation of the Vereos PET/CT system according to the NEMA NU2-2012 standard. *J Nucl Med.* 2019;60:561–567.
13. Hsu DFC, Ilan E, Peterson WT, Uribe J, Lubberink M, Levin CS. Studies of a next-generation silicon-photomultiplier-based time-of-flight PET/CT system. *J Nucl Med.* 2017;58:1511–1518.
14. van Sluis J, de Jong J, Schaar J, et al. Performance characteristics of the digital Biograph Vision PET/CT system. *J Nucl Med.* 2019;60:1031–1036.
15. Tsutsui Y, Awamoto S, Himuro K, Kato T, Baba S, Sasaki M. Evaluating and comparing the image quality and quantification accuracy of SiPM-PET/CT and PMT-PET/CT. *Ann Nucl Med.* 2020;34:725–735.
16. Wagatsuma K, Miwa K, Sakata M, et al. Comparison between new-generation SiPM-based and conventional PMT-based TOF-PET/CT. *Phys Med.* 2017;42:203–210.
17. Surti S, Viswanath V, Daube-Witherspoon ME, Conti M, Casey ME, Karp JS. Benefit of improved performance with state-of-the art digital PET/CT for lesion detection in oncology. *J Nucl Med.* 2020;61:1684–1690.
18. Fukukita H, Suzuki K, Matsumoto K, et al. Japanese guideline for the oncology FDG-PET/CT data acquisition protocol: synopsis of version 2.0. *Ann Nucl Med.* 2014;28:693–705.
19. Hashimoto N, Morita K, Tsutsui Y, Himuro K, Baba S, Sasaki M. Time-of-flight information improved the detectability of subcentimeter spheres using a clinical PET/CT scanner. *J Nucl Med Technol.* 2018;46:268–273.
20. Akamatsu G, Ikari Y, Nishida H, et al. Influence of statistical fluctuation on reproducibility and accuracy of SUVmax and SUVpeak: a phantom study. *J Nucl Med Technol.* 2015;43:222–226.